Research on Engineering Structures & Materials
www.jresm.org
MIM Research Group

Research Article

Numerical study of stiffness degradation and dissipated energy in early cyclic behavior of non-conforming RC beam–column joints

Mohamed Mimouni [*,1,3,a], Djamel El Ddine Kerdal [2,b], Lamia Kharroubi [1,3,c]

[1]*Civil Engineering Department, U.S.T.O.M.B., B.P. 1505 El M'Naouer, Oran, Algeria*
[2]*LM2SC, Civil Engineering Department, U.S.T.O.M.B., B.P. 1505 El M'Naouer, Oran, Algeria*
[3]*Laboratoire Matériaux et Structures, Civil Engineering Department, University of Tiaret, Zaaroura, B.P. 78, Tiaret, Algeria*

Article Info

Article History:

Received 02 Nov 2025

Accepted 06 Feb 2026

Keywords:

RC Beam–column joints;
Non-conforming;
Initial cycles;
ANSYS;
Stiffness degradation;
Energy dissipation;
Hybrid index

Abstract

Beam-column joints are critical components influencing the seismic performance of reinforced concrete (RC) frames, especially in regions with moderate to high seismic activity. A significant proportion of Algeria's building stock was constructed before 1980, prior to the adoption of the Algerian seismic regulations, resulting in inadequate seismic detailing and making these joints especially vulnerable to earthquakes. This study examines the impact of initial cycles of lateral load on the seismic performance of non-conforming external reinforced concrete beam-column joints, focusing on early stiffness degradation and energy dissipation processes. A three-dimensional nonlinear finite element model was created in ANSYS and compared with experimental data from the literature, confirming the accuracy of the numerical method. The originality of this work resides in the infrequently studied correlation between stiffness loss and energy dissipation, illustrated by a normalized dual-curve representation. This approach helps the identification of a pivotal intersection point that signifies the threshold of post-elastic behavior. A hybrid index (D_{Hybrid}) is proposed, incorporating these two parameters into a singular synthetic indicator for the preliminary evaluation of seismic performance. A detailed parametric analysis was performed to investigate the impact of critical variables such as concrete compressive strength, beam longitudinal reinforcement ratio, and joint core confinement. The findings indicate that the early loading cycles are crucial in initiating stiffness degradation and cumulative energy dissipation, determining the beginning of nonlinear behavior, and substantially affecting the seismic response of nonconforming joints.

1. Introduction

Algeria is one of the most seismically active countries in the Mediterranean due to the convergence between the African and Eurasian plates. Past earthquakes, such as the 1980 El-Asnam (moment magnitude, M_w 7.3) and the 2003 Boumerdès (M_w 6.8), have highlighted the high vulnerability of existing reinforced concrete frame buildings, particularly at beam–column joints [1]. This vulnerability is not limited to Algeria but is observed worldwide, where many RC buildings were built prior to the adoption of modern seismic codes and the capacity design philosophy. Such structures often exhibit inadequate detailing, which significantly compromises the seismic performance of beam–column joints, leading to rapid stiffness degradation and limited energy dissipation under seismic loading [2, 3]. Numerous catastrophic structural failures reported in past earthquakes have been attributed to the poor performance of RC beam–column joints. Post-

*Corresponding author: mimouni_gc@yahoo.fr
[a]orcid.org/0009-0008-5578-3491; [b]orcid.org/0000-0001-9599-1393; [c]orcid.org/0009-0003-1796-3014
DOI: http://dx.doi.org/10.17515/resm2026-1316st1102rs

earthquake reconnaissance missions consistently show that damage is frequently concentrated in these joints, often resulting in partial or total collapse of RC frame systems [1, 4, 5].

In view of these deficiencies, substantial research has been conducted in the past few decades to enhance the understanding of non-ductile reinforced concrete beam-column joints and to design appropriate assessment and retrofit methodologies. Pioneering research from the 1980s, by Durrani and Wight [6] and Ehsani and Wight [7], showed that the number of joint stirrups, joint shear stress, and the presence of transverse beams affect stiffness degradation, energy dissipation, and the overall seismic performance of reinforced concrete beam-column joints. Subsequent investigations of gravity-load-designed sub assemblages [8, 9] demonstrated flexure-dominated damage, insufficient ductility, and significant column failures, affirming the critical influence of lap splice location, joint reinforcement, and bar anchorage. Pampanin et al. [1] examined joints characteristic of 1950s–1970s construction, characterized by smooth bars, absence of transverse reinforcement, and insufficient anchorage, revealing panel-zone vulnerability, stiffness loss due to bar slip, and brittle "concrete wedge" failures in external joints. Clyde et al. [10] and Pantelides et al. [2] proved the seismic vulnerability of these joints, illustrating that insufficient anchoring led to bond-slip and pinching, while increased axial load somewhat improved shear strength but reduced ductility and accelerated stiffness degradation. These results led to an extensive amount of research on ways to retrofit. RC or Carbon Fiber Reinforced Polymer CFRP jacketing effectively converted brittle shear failures into ductile beam hinging, significantly improving energy dissipation [11, 12]. Kuang and Wong [13] illustrated how important beam bar anchorage is for joint shear strength and hysteretic response. Testing on real joints from a building that was damaged in the 2009 L'Aquila earthquake revealed that FRC jacketing stopped joint shear failure, modified the response to beam yielding, and significantly enhanced shear strength and energy dissipation [14].

Recent studies have concentrated on new retrofitting and design strategies for non-seismic reinforced concrete joints. Sonawane and Dubey [15] noted that rectangular spiral reinforcement significantly enhanced crack control, ductility, and energy dissipation in comparison to traditional stirrups. Shaaban and Seoud [16] demonstrated that the combination of ferrocement layers with steel angles significantly enhances stiffness retention, energy dissipation, and ductility under cyclic loading. Lim et al. [17] have shown that incorporating a CFRP grid into engineered cementitious composite (ECC) enhances crack control, ductility, and energy dissipation relative to high-strength mortar or retrofitted specimens. Araby et al. [18] augmented gravity-load-designed joints using ferrocement layers, demonstrating considerable enhancements in deformation capacity, stiffness, and energy dissipation, while exhibiting no notable change in ultimate strength. Following these trends, Helal et al. [19] used post-tensioned metal straps to reduce the loss of stiffness and increase strength and energy dissipation. Similarly, Golias and Karayannis [20] used X-shaped near-surface mounted NSM Carbon Fiber Reinforced Polymer C-FRP ropes to get strength gains of up to ~65% and energy dissipation gains of up to three times.

In addition to experimental research, various analytical formulations have been created to analyze the cyclic behavior of RC beam-column joints. Paulay and Priestley [21] developed significant formulations for joint shear strength and ductile detailing that became the basis for many models developed after them. Biddah and Ghobarah [22] and Hwang and Lee [23] established models that included joint shear deformation, bond-slip effects, and softened strut-and-tie mechanisms, and they were tested against large sets of experimental data. Pantelides et al. [2] tested six full-scale exterior joints with inadequate reinforcement details. They evaluated load capacity, drift, shear strength, and ductility under two levels of axial load. They proposed and approved limit-state and strut-and-tie models to forecast the failure mechanisms of joints designed for gravity loads. Lowes et al. [24] created a four-node joint element that was added to OpenSees. It modeled bar slip, panel shear, and interface shear degradation, and it was tested against a lot of experimental data. Mitra and Lowes [25] modified this model by incorporating diagonal strut shear formulation and an improved bar-slip representation, resulting in increased precision in illustrating stiffness and strength degradation under cyclic loading. Celik and Ellingwood [26] and Park and Mosalam [27] complemented these developments with calibrated models for joints without transverse reinforcement and for fragility assessment, whereas Le-Trung et al. [28] applied analytical modeling to CFRP-strengthened connections, precisely predicting stiffness degradation and energy dissipation. LaFave and Kim [29] collected 341 joint tests and created Bayesian shear strength and deformation models that highlight the impact of joint aspect ratio, confinement, and concrete strength, outperforming code-based equations and enabling mechanism-based joint modeling.

Recent research has concentrated on the advancement of advanced macro-elements and retrofit-oriented modeling to enhance predictive accuracy and computational efficiency. Mosallam et al. [30] used analytical and nonlinear numerical modeling to evaluate FRP-retrofitted joints, showing substantial enhancements in strength, stiffness retention, and energy dissipation. Pantò et al. [31] reinforced this trend by introducing the "Joint with Hinges" macro-element, which can reproduce panel shear, bar slip, and plastic hinge formation in one framework. Simultaneously, Gombosuren and Maki [32] created simpler predictive equations for joint shear deformation indices. These equations are useful for finding inelastic joints without having to do a full nonlinear analysis. Grande et al. [33] developed a nonlinear macro-model derived from the "scissors model," calibrated in OpenSees, to simulate pinching and cyclic degradation phenomena. The latest works by Irreño Palomo et al. [34] and Kalogeropoulos et al. [35] integrated analytical and numerical methods for Ultra-High Performance Fiber Reinforced Concrete (UHPFRC) UHPFRC-jacketed and deficient joints, respectively, precisely replicating stiffness degradation, energy dissipation, and failure mechanisms under cyclic loading.

In general, these analytical studies reveal how approaches have evolved, from local shear models to more comprehensive macro-models. This data shows how advanced this field of research has become. The first numerical methods used simplified macro-models to make frame-level simulations cheaper to run. Lowes and Altoontash [24] developed a joint element in OpenSees that combines a shear panel and bar-slip springs. This element shows how stiffness and strength change under cyclic loading. Mitra and Lowes [25] modified this formulation by incorporating a confined-concrete shear strut and refining hysteretic rules to more accurately simulate pinching and energy dissipation. These advancements formed the basis for subsequent finite element modeling, prompting a shift towards more detailed 3D simulations capable of representing localized cracking, bond-slip phenomena, and joint shear stress distributions.

Researchers gradually adopted detailed 3D nonlinear finite element method (FEM) simulations to enhance the depiction of joint mechanics. Goto and Joh [36] combined cyclic tests with DIANA analyses to observe shear cracking caused by eccentricity and a reduction in stiffness after the peak. Ibrahim and Elbadry [37] validated ATENA 3D models for joints reinforced with double-headed studs, replicating hysteretic loops and proving their ductile behavior. Eslami et al. [38] utilized ANSYS to illustrate that CFRP retrofitting can move plastic hinges to beams and establish a strong-column weak-beam mechanism, increasing the estimated seismic capacity from 0.37g to 0.45g. Baji et al. [39] utilized VecTor2 to forecast load–displacement responses and failure modes of FRP-strengthened joints beyond experimental thresholds. Further research by Venkatesan et al. [40] and Laseima et al. [41] used ANSYS simulations and cyclic tests together to show that ferrocement or FRP strengthening increases moment capacity and cumulative energy dissipation (up to 200%) and delays stiffness loss. Al-Rousan and Alkhawaldeh [42] extended this study by explicitly simulating FRP–concrete bond degradation in ANSYS, demonstrating that bond deterioration under 30% continues to enhance ductility and retard stiffness loss.

Recent studies have concentrated on advanced materials, hybrid methodologies, and machine-learning-enhanced predictions. Kytinou et al. [43] employed full-scale tests and complete Abaqus models to verify the seismic performance of CFRP-reinforced joints, precisely predicting bar slip and hysteretic loops. Fayaz et al. [44] numerically illustrated in Abaqus that the combination of UHPFRC and CFRP retrofitting results in a 2.6-fold increase in peak load and considerably postpones the deterioration of strength and stiffness. Marie et al. [45] established a machine learning framework [(Ordinary Least Squares (OLS), Support Vector Machines (SVM), K-Nearest Neighbour Regression (KNN), Multivariate Adaptive Regression Splines (MARS), Artificial Neural Networks (ANN), Kernel Regression with mixed data types (Kernel)] that reached an R^2 value of 0.9752 for predicting shear strength, providing a cost-effective substitute for complicated simulations. Zhuang et al. [46] employed OpenSees fiber models to examine prefabricated FRC joints featuring grouted sleeves, suggesting optimal shear-span ratios ranging from 2.0 to 2.5. In 2025, Sayed Ahmed et al. [47] demonstrated the efficacy of steel-angle retrofits through 3D finite element modeling. Concurrently, Maulana et al. [48] and Sabbahfar et al. [49] confirmed the DIANA and ATENA 2D models on non-ductile interior joints, successfully capturing crack propagation, hysteresis loops, and stiffness degradation. Furthermore, Prakash and Parthasarathi [50] used both Complete Abaqus Environment (Abaqus/CAE) simulations and ANN regression to test FRP-rehabilitated joints at high temperatures. They found that CFRP laminates were the best for thermal and mechanical strength.

The critical review of experimental, analytical, and numerical studies highlights significant advances in understanding the seismic behavior of RC beam–column joints, yet underscores a lack of focused research on the early degradation phase and on the correlation between stiffness loss and energy dissipation in such joints.

The current study is part of a larger research project aimed to investigate the seismic strength of existing RC buildings, with a focus on the exterior beam-column joints in Algerian buildings constructed before 1980. These joints often lack adequate seismic detailing, which makes them very likely to be damaged by earthquakes. More specifically, this work examines the early behavior under reversed lateral loading, which is a phase characterized by significant stiffness degradation that primarily affects the subsequent structural response. Unlike most existing studies that analyze beam–column joint behavior until failure, this research concentrates on the onset of degradation, a critical phase for forecasting structural vulnerability. Its originality resides in the establishment of a direct correlation between stiffness loss and cumulative energy dissipation via a normalized dual-curve representation, a topic rarely addressed concurrently in existing literature. This method shows a key point where post-elastic behavior starts. A hybrid index (D_{Hybrid}) is also suggested, which combines normalized residual stiffness and cumulative energy dissipation into one measurable indicator for early damage assessment.

The created three-dimensional nonlinear finite element model, which was validated against experimental data in ANSYS [51], allows for accurate tracking of stiffness degradation and energy dissipation at each cycle. This provides new insights into the vulnerability of RC joints to seismic activity. A detailed parametric analysis subsequently examines the influence of important factors such as concrete compressive strength, beam longitudinal reinforcement ratio, and joint core confinement on energy dissipation and stiffness degradation. The results reveal the factors influencing initial degradation under cyclic loads and offer a practical instrument for evaluating seismic vulnerability.

2. Materials and Modelling Procedure

2.1. Finite Element Modelling of Exterior RC Beam-Column Joints

Using ANSYS [51], a three-dimensional nonlinear finite element (FE) model was created to simulate the cyclic behavior of RC exterior beam-column joints. The modeled joint subassembly accurately reproduced the geometry and reinforcement details of the experimental specimen. The Solid65 element, an eight-node brick with three translational degrees of freedom per node, was used to model concrete. It could simulate both tensile cracking and compressive crushing. We used a multi-linear stress-strain curve, the Von Mises yield criterion, and the Willam-Warnke failure model to define how the concrete would behave. This work was done to show how it would respond and fail in a nonlinear way [52]. Shear transfer coefficient is taken 0.25 for open cracks and 0.99 for closed cracks [51, 53].

LINK8 truss elements, each with two nodes and three translational degrees of freedom, were used to show the steel reinforcement in the beams and columns. A multi-linear kinematic hardening model (MKIN) was used to reproduce the inelastic steel response. This model utilized parameters such as elastic modulus, yield strength, and tangent modulus [53]. Even though bond-slip between concrete and reinforcement significantly influences joint behavior, this study assumed that there was a perfect bond. To satisfy this assumption, reinforcement elements were connected to adjacent concrete solid elements by sharing common nodes, thus enabling full interaction between concrete and steel.

The finite element model was developed based on the test specimen RCNH1, selected from the literature (Figure 1). This specimen was part of an experimental program on exterior RC beam–column joints conducted by Gencoglu and Mobasher [54]. In the nonlinear analysis, the total load was applied incrementally, and the solution was obtained using the modified Newton–Raphson method [51]. Appropriate boundary conditions and loading were defined to replicate the experimental setup. Taking advantage of the symmetry in both geometry and loading, only half of the joint was modeled in the finite element analysis (FEA), which considerably reduced computational time and memory requirements. In the numerical model, Solid45 elements were used to simulate the steel loading plates. The nodes of these steel elements were connected to those of the adjacent concrete elements (Solid65) to satisfy the perfect bond assumption.

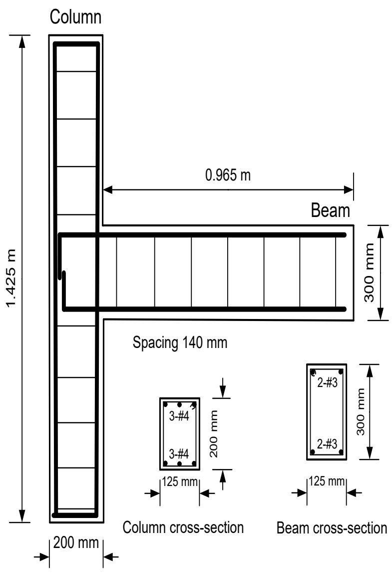

Fig. 1. Geometry and reinforcement details of exterior beam–column joint specimen RCNH1 [54]

The RCNH1 specimen was a half-scale exterior joint designed to replicate the characteristics of older RC structures with poor seismic detailing. The beam was 125 mm × 300 mm in cross-section, and the column was 125 mm × 200 mm. The longitudinal reinforcement of the beam penetrated 200 mm into the joint. The joint region didn't have any transverse reinforcement, which is a common problem seen in pre-code construction.

The specimen was constructed using concrete with a compressive strength of 30 MPa. The longitudinal reinforcement was made of Grade 60 steel bars (yield strength ≈ 525 MPa), and the stirrups were made of Grade 40 steel bars (yield strength ≈ 290 MPa). The column had a constant axial load of 90 kN on it, which is about 13% of its axial capacity (0.13 Ag f'c). Reversed cyclic lateral loading was simulated in ANSYS under displacement control. Alternating positive and negative displacement cycles with progressively increasing amplitudes were applied at the beam free end using APDL tabular functions. This loading history reproduced the experimental protocol slowly imposed by a 250 kN Mechanical Testing Systems (MTS) actuator [54].

2.2. Experimental Validation of the Finite Element Model

To validate the accuracy of the developed numerical model, the experimental specimen RCNH1, tested at Arizona State University, was adopted as a benchmark reference. This specimen, reported by Gencoglu and Mobasher [54], represents a non-conforming exterior RC beam–column joint subjected to reversed cyclic loading. Since the original experimental data were not publicly available, representative points were extracted from the published hysteresis curves using a digitization tool to reproduce the overall cyclic response for model validation.

Figure 2 presents the cyclic load–displacement response at the beam tip, comparing the experimental data of specimen RCNH1 with the finite element (FE) simulation. The experimental loops (in black) exhibit the typical pinching effect and progressive stiffness degradation resulting from bond-slip and shear damage in the unconfined joint core. Conversely, the simulated loops (in red) display a fuller hysteretic shape with a less pronounced pinching behavior, especially at larger displacement amplitudes.

The numerical model constructed with ANSYS properly represents the seismic behavior of RC beam-column connections, particularly for the load-displacement envelope, peak strength, and stiffness progression. The initial loading cycles are captured with sufficient accuracy to enable a reliable analysis of stiffness deterioration and energy dissipation, which are the primary focuses of this study. The hysteresis loops generated by the simulation appear fuller and exhibit reduced pinching compared to those observed in experiments. This reaction aligns with conventional finite element modeling techniques that do not explicitly incorporate bond-slip effects and progressive local degradation. As previously highlighted by Ronagh and Baji [55], this modeling simplification does not significantly compromise the model's ability to provide reliable predictions for assessing the seismic vulnerability of existing joints during the early phases of cyclic loading.

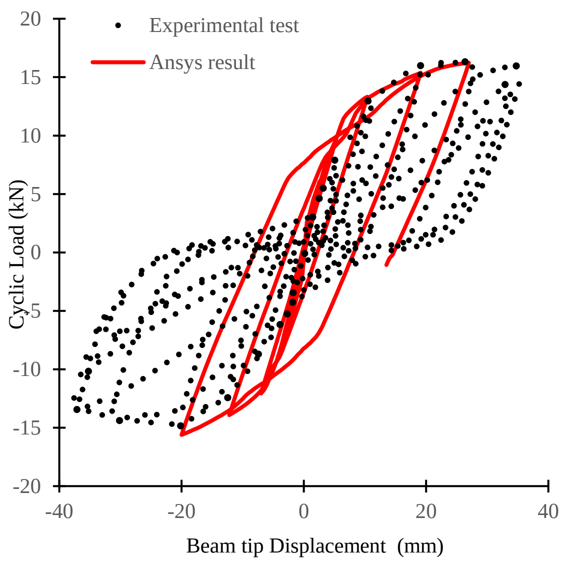

Fig. 2. Comparison of cyclic load–displacement responses between FE simulation (ANSYS) and experimental results for specimen RCNH1 [54]

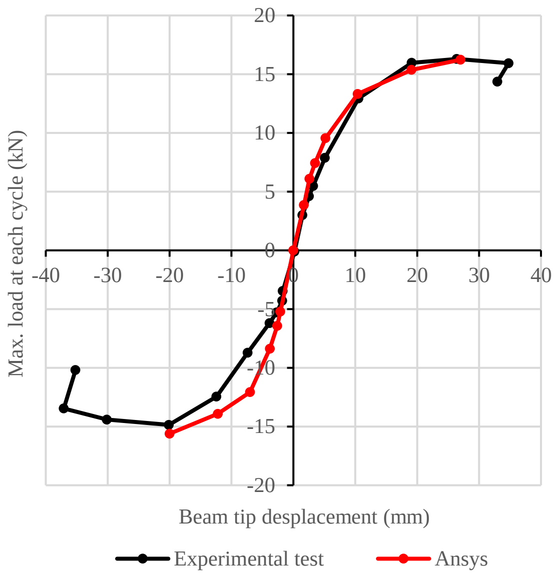

Fig. 3. Comparison of load–displacement backbone curves from the experimental test [54] and the FE simulation (Ansys)

The curve in Figure 3 shows the maximum cyclic load attained by both the finite element (FE) model (ANSYS) and the experimental specimen RCNH1 at each displacement level. In general, the two responses are in good agreement. The general shape and trend of the load–displacement backbone curves are well reproduced, confirming the model's ability to accurately capture early stiffness degradation and the nonlinear cyclic behavior of RC joints.

2.3. Modeling of Pre-Code Non-Conforming RC Joints in Algerian Buildings

After validating the initial numerical framework, a finite element model was developed to analyze the seismic response of RC exterior beam–column joints representative of typical Algerian buildings constructed in 1971. These joints commonly exhibit inadequate detailing practices, including smooth longitudinal bars, inadequate anchorage, no transverse reinforcement in the joint core, and poor confinement conditions. All of these factors make them significantly more likely to fail when they are loaded laterally. This numerical model serves as the foundation for a parametric study designed to quantify the impact of critical design parameters, such as concrete compressive strength and longitudinal and transverse reinforcement ratios, on seismic behavior in the early stages. We put a lot of focus on assessing stiffness degradation and hysteretic energy dissipation during the first loading cycles. These are important signs of when structural damage starts and how it becomes worse.

Figure 4 illustrates the geometry and size (in cm) of the modeled specimen for the numerical analysis using ANSYS [51] to simulate the RC exterior beam-column joint. The appropriate element types and material properties used in the model are described below.

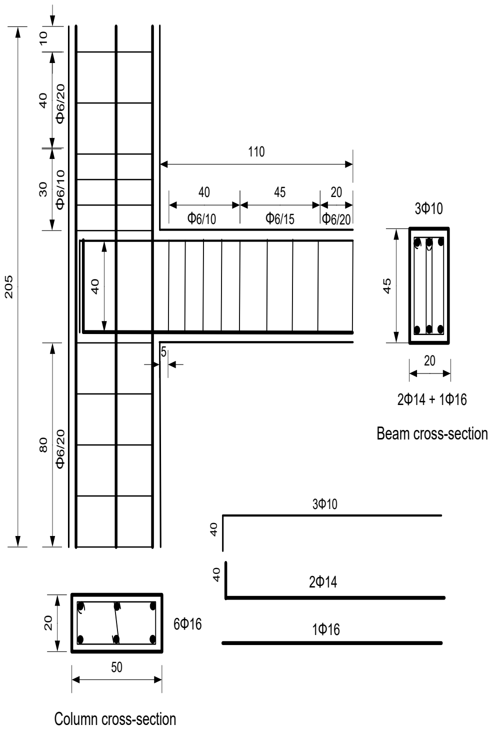

Fig. 4. Overall geometry and dimensions of the modeled RC beam–column joint (in cm)]

The material properties of concrete and reinforcement adopted for the numerical modeling of the beam–column joints are summarized in Tables 1 and 2.

Table 1. Concrete material properties

Compressive strength, f_c' (MPa)	Tensile strength, f_t (MPa)	Young's modulus E_s (MPa)
30	2.4	32164.19

Table 2. Reinforcement material Properties

Reinforcement	Yield strength, f_y (MPa)	Young's modulus, E_s (GPa)
Longitudinal reinforcement	400	200
Transverse reinforcement	240	200

The FE model using ANSYS [51] was analyzed under reversed cyclic lateral loading. Figure 5 shows the stress–strain relationship of concrete, modeled using the Multilinear Isotropic Hardening option, based on the approach proposed by Kachlakev et al. [53]. The stress–strain relationship for reinforcing steel is defined as a bilinear model, assumed to be elastic–perfectly plastic, as illustrated in Figure 6. A perfect bond between concrete and steel reinforcement was assumed. The steel reinforcement was connected to the nodes of each adjacent concrete solid element, so that both materials shared common nodes, ensuring full interaction.

The finite element mesh of the beam–column model is shown in Figure 7. A uniform element size of 25 mm was adopted, as it ensured a satisfactory compromise between numerical convergence stability and computation time. Due to symmetry in both geometry and loading, only half of the width of the model was represented in the finite element analysis (FEA). Cyclic bending was applied at the free end of the beam to simulate the effect of a severe earthquake (Figure 8). The load was applied at a distance of 5 cm from the free end of the beam, through steel plates.

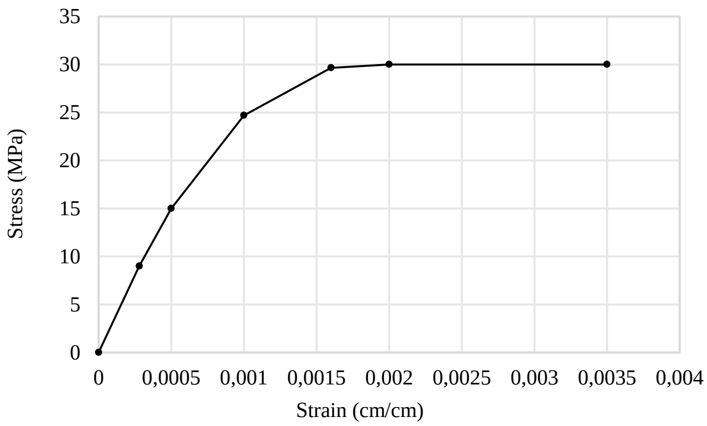

Fig. 5. Idealized stress-strain curve of concrete

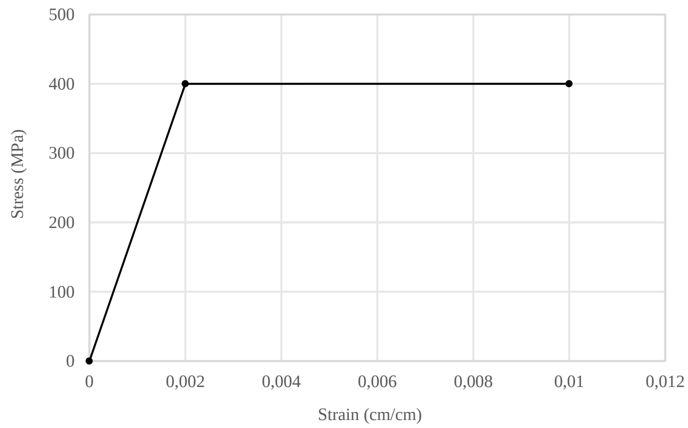

(a)

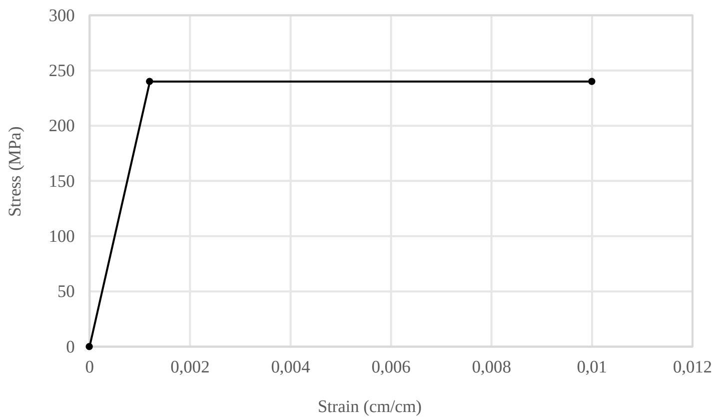

(b)

Fig. 6. Idealized stress-strain curves of reinforcing steel (a) Longitudinal reinforcement (b) Transverse reinforcement

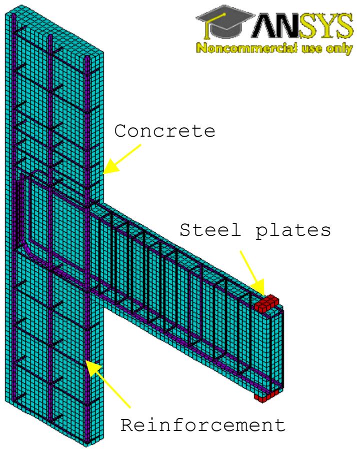

Fig. 7. Mesh of the concrete, steel plate, and steel support

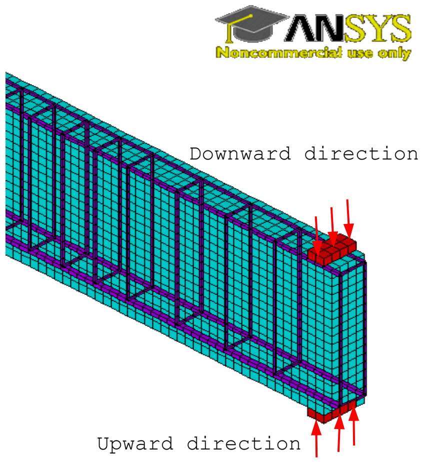

Fig. 8. Application of cyclic loading through steel plates

The boundary conditions were defined at the plane of symmetry and at the ends of the columns. The displacements of the nodes at the top of the columns were constrained to zero in all three directions. With respect to the plane of symmetry located in the XY plane, the Z-displacement of the nodes lying on this plane was also set to zero.

3. Results and Discussion

3.1 Hysteretic Moment–Rotation Response from FE Simulation

Figure 9 illustrates the moment–rotation hysteresis curve. It displays a steep initial elastic segment, then the stiffness decreases and the hysteresis loops become wider, signifying cumulative energy dissipation. There is a clear difference between the positive and negative branches, caused by the uneven distribution of longitudinal reinforcement (3Ø10 at the top of the beam vs. 2Ø14 + 1Ø16 at the bottom). The joint reached a maximum moment of 106 kN.m at a rotation of 0.0072 rad in the upward direction and 60.2 kN.m at 0.0085 rad in the downward direction, beyond which convergence failure occurred due to excessive cracking.

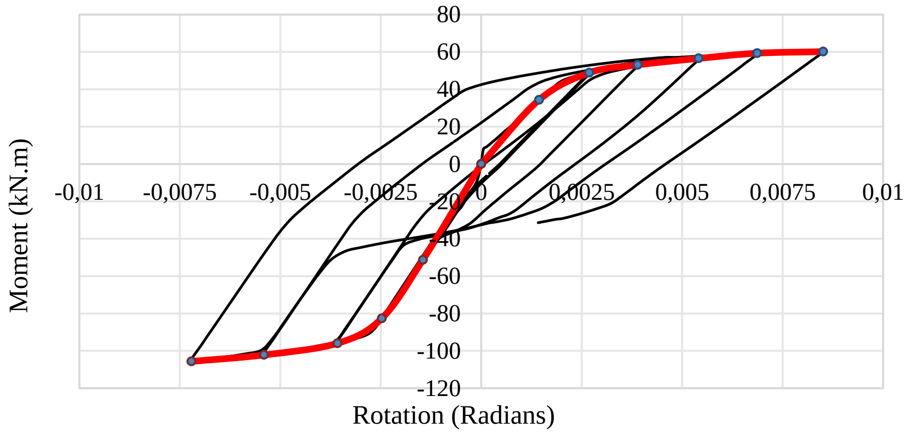

Fig. 9. Moment-rotation hysteresis curve of the RC joint obtained from Ansys

3.2 Stiffness and Energy Dissipation Characteristics

In seismic studies of reinforced concrete structures, two aspects are often examined to understand how beam–column joints behave under cyclic loading: the loss of stiffness and the ability to dissipate energy. The gradual reduction in stiffness reflects how the joint becomes less rigid as loading cycles progress, while energy dissipation describes its effectiveness in absorbing and releasing the input energy through the hysteretic response of the materials.

The degradation of stiffness was evaluated cycle by cycle through the peak-to-peak stiffness K_{pp}. This parameter corresponds to the slope of the secant line connecting the maximum and minimum moment points on the moment–rotation hysteresis loop for each cycle [35, 56]. The energy dissipated per cycle is quantified by the area enclosed within the moment–rotation hysteresis loop [17, 18]. The results summarized in Table 3 and illustrated in Figures 10 to 12 present the combined evolution of peak-to-peak secant stiffness and energy dissipation.

Table 3. Evolution of stiffness degradation and cumulative energy dissipation during early cyclic loading

Cycles	Peak to Peak Stiffness K_{pp} (kN.m/rad)	Normalised stiffness degradation (K_{norm})	Energy dissipation E_d (N.m)	Cumulative energy dissipation $E_{d,cum}$ (N.m)	Normalised cumulative Energy (E_{norm})
1	29632.82	1	9.81	9.81	0.0047
2	25474.38	0.86	34.40	44.21	0.0212
3	19948.88	0.67	145.00	189.21	0.0908
4	14674.85	0.49	359.00	548.21	0.2631
5	11717.11	0.39	602.00	1150.21	0.5520

From the first loading cycles, the stiffness starts to reduce: the peak-to-peak stiffness decreases from 29632.82 kN.m/rad in the first cycle to 25474.38 kN.m/rad in the second, corresponding to a 14% reduction. This degradation continues to occur at different levels of intensity until it reaches 11717.11 kN.m/rad by the fifth cycle. This decline corresponds to a total loss of more than 60%, as shown in Table 3, Figures 10 and 11.

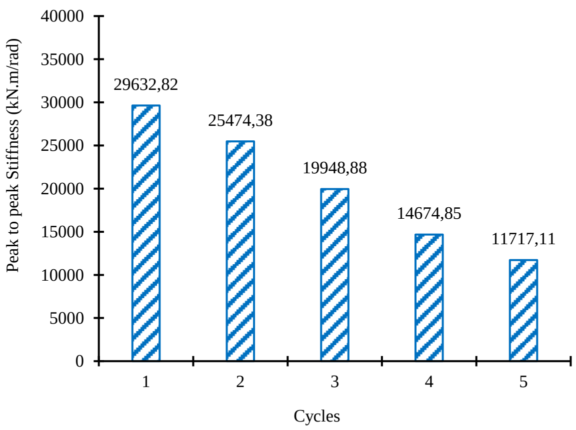

Fig. 10. Peak to peak stiffness degradation during early cyclic loading

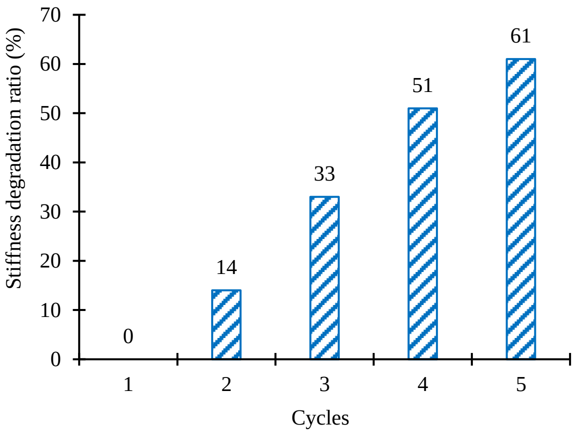

Fig. 11. Evolution of stiffness degradation ratio during early cyclic loading

At the same time, energy dissipation stays relatively small in the beginning, with only 9.81 N.m and 34.40 N.m dissipated in the first and second cycles, respectively. This indicates that the initial hysteretic energy absorption capacity is limited. From the third cycle on, there is a significant increase, and by the fifth cycle, it reaches 602 N.m, as shown in Table 3. This behavior shows that large inelastic deformations are starting to happen, marking the transition of the joint into a nonlinear response regime.

As illustrated in Table 3, the normalized stiffness degradation (K_{norm}) is defined as the ratio K_i/K_0, where K_0 denotes the initial reference stiffness evaluated from the first loading cycle. In parallel, the normalized cumulative energy dissipation (E_{norm}) is given by the ratio $E_{cum,i}/E_{ref}$, with E_{ref} corresponding to the cumulative energy dissipated at the end of the analysis.

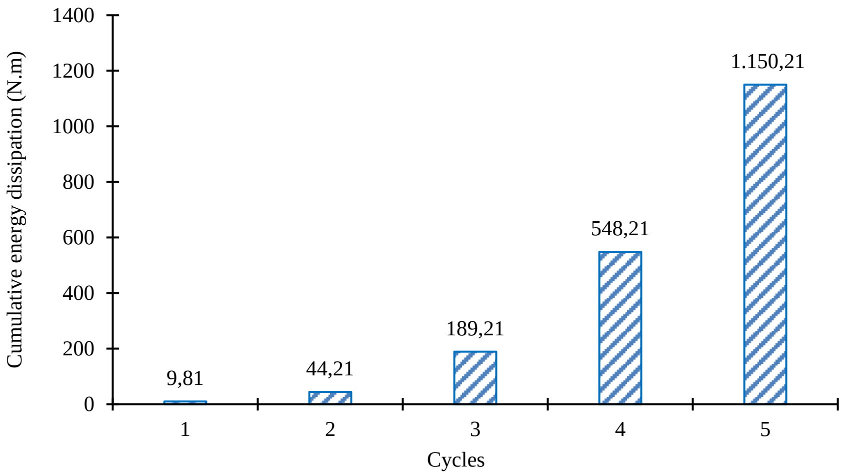

Fig. 12. Cumulative energy dissipation during early cyclic loading

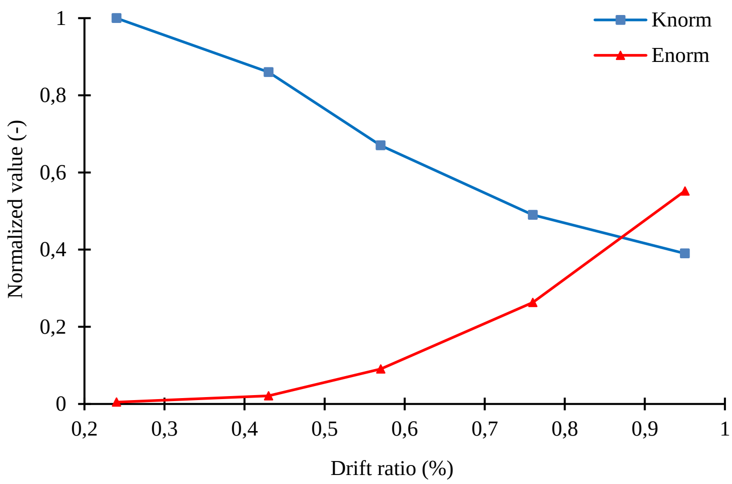

Fig. 13. Evolution of normalized stiffness degradation and cumulative energy dissipation during early cyclic loading

Figure 13 shows how normalized stiffness degradation (K_{norm}) and normalized cumulative energy dissipation (E_{norm}) change as drift (%) changes. There is a clear inverse relationship: as drift increases through the first five loading cycles, stiffness decreases and energy dissipation, which was low at first, rises sharply at higher drift levels.

The normalized stiffness degradation (K_{norm}) is equal to its reference value (1.00) at cycle 1, which corresponds to a drift of 0.24%. The normalized cumulative energy dissipation (E_{norm}), on the other hand, is almost zero, or close to 0%. At cycle 2 (0.43% drift), the normalized stiffness decreases to 0.86, reflecting a reduction of approximately 14%. Energy dissipation stays low, though, making up only about 2% of the total cumulative energy at the end of the analysis. At cycle 3, the drift reaches 0.57%, and the normalized stiffness exhibits a further reduction to 0.67, corresponding to a loss of about 33%. The normalized cumulative energy, on the other hand, increases to about 9%. At this point, inelastic mechanisms start to work, and the material moves out of the elastic range. The degradation grows worse at a drift of 0.75% (cycle 4) and 0.95% (cycle 5): the stiffness diminishes to 0.49 and 0.39, respectively, amounting to a total decrease of about 61 %. At the same time, normalized energy dissipation speeds up quickly, reaching 26% and 55% of the total cumulative energy.

This contrasting evolution underscores the gradual involvement of energy-dissipating mechanisms in a low-ductility RC joint. Previous research has frequently examined stiffness degradation and energy dissipation in isolation; however, the novelty of the current study resides in the direct correlation of these two mechanical responses via a dual normalized-curve representation. The intersection of the two normalized curves, seen in the drift range of 0.75% - 0.95% (cycles 4 and 5) at a normalized value of about 0.45, may be a key point where energy dissipation becomes more important than stiffness, marking the shift from serviceability to damage. The combined normalized-curve approach is unique to this study; however, analogous mechanical behaviors have been documented in experimental research. Tsonos et al. [57] specifically noted that RC joints constructed per outdated code provisions demonstrate significant stiffness degradation, while their energy dissipation capacity is restricted during initial loading phases, unlike well-detailed joints that preserve a more consistent hysteretic response.

3.3 Hybrid Index Linking Stiffness Degradation and Energy Dissipation

In this section, we propose the D_{Hybrid} index, which combines the evolution of normalized stiffness loss (K_{norm}) and normalized energy dissipation (E_{norm}). It is inspired by the work of Park and Ang [58], who related ultimate deformation to hysteretic energy dissipation for the evaluation of seismic damage. Unlike this formulation, which depends on ultimate deformation unobservable during the early cycles, the present approach replaces it with normalized stiffness loss while preserving the contribution of cumulative energy dissipation. By construction, the index remains bounded between 0 (undamaged) and 1 (fully damaged), thereby providing a simple and directly applicable tool for assessing early-stage damage in RC beam–column joints subjected to cyclic seismic loading. At cycle *i*, the hybrid damage index is defined as:

$$D_{Hybrid}(i) = \alpha_i.(1 - \frac{K_i}{K_0}) + (1 - \alpha_i).(\frac{E_{cum,i}}{E_{ref}}) \quad (1)$$

Where; K_i : the secant stiffness at cycle i; K_0 : the reference stiffness (initial tangent or first-cycle secant); $E_{cum,i}$: the cumulative hysteretic energy up to cycle i; E_{ref}: a common energy reference. The adaptive coefficient, denoted as α_i, is expressed as follows:

$$\alpha_i = \frac{(1 - \frac{K_i}{K_0})}{(1 - \frac{K_i}{K_0}) + (\frac{E_{cum,i}}{E_{ref}})} \quad (2)$$

The normalized stiffness degradation at the cycle "i" is represented by the value of K_i/K_0, while the normalized cumulative hysteretic energy dissipation is represented by the value of $E_{cum,i}/E_{ref}$. Thus, the adaptive coefficient α_i evolves depending on whether stiffness degradation or energy dissipation predominates, ensuring a balanced contribution within the hybrid index.

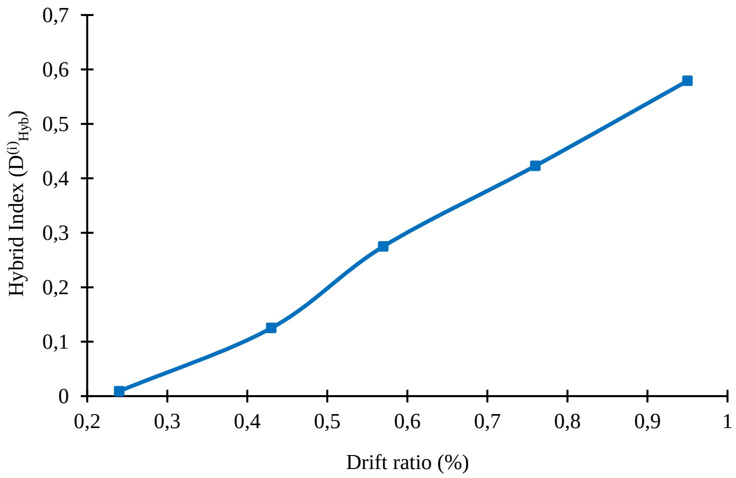

Fig. 14. Evolution of hybrid index (D_{Hybrid}) vs. drift ratio (%) during early cyclic loading

Figure 14 shows how the proposed hybrid index (D_{Hybrid}) changes over the first five loading cycles as the drift ratio changes. The proposed index exhibits a gradual rise with increasing drift, reflecting the combined effects of stiffness degradation and cumulative energy dissipation. During the first loading cycle, at a drift ratio of about 0.24%, its value grows only slightly from 0.009 to 0.125, indicating that the response remains essentially quasi-elastic with negligible hysteretic losses. The index rises more noticeably between the second (0.43%) and third (0.57%) cycles, reaching almost 0.275. This phase is the beginning of inelastic behavior, which is marked by a clear drop in stiffness and an increase in energy dissipation. After the third cycle, the evolution becomes more stable and follows a more linear path. It goes from about 0.35 at the fourth cycle (0.76%) to about 0.58 at the fifth (0.95%). This pattern shows that the index can pick up on early-stage degradation and show when RC beam-column joints go from elastic to inelastic response. The drift range observed in this study, attaining a moderate value of 0.95%, highlights substantial early-cycle damage. The (D_{Hybrid}) index offers an objective assessment of degradation and serves as a foundation for the parametric analysis of critical parameters in their cyclic response.

4. Parametric Study

The studied parameters are the concrete compressive strength, the beam longitudinal reinforcement ratio, and the transverse reinforcement ratio within the joint core. A 3D nonlinear finite element analysis in ANSYS was conducted to assess their influence on joint performance in terms of stiffness degradation, cumulative energy dissipation, and the hybrid index (D_{Hybrid}). The analysis focuses on the first five loading cycles, which capture early inelastic mechanisms.

4.1 Effect of Concrete Compressive Strength: f’c

This parametric study first examines the influence of concrete compressive strength (f’c) on stiffness degradation and energy dissipation during the first few loading cycles. Three strength levels are considered: 30, 40, and 60 MPa.

Figure 15 shows how the stiffness degradation ratio ($1-(K_i/K_0)$) increases in the first five loading cycles for all concrete strengths. Higher f'c variants show a faster degradation in the early cycles. This is because the initial stiffness is higher and the unconfined joint core is brittle when it shears. But by cycle 5, the curves come together at about 61–63% degradation, which shows that the effect of f'c disappears quickly.

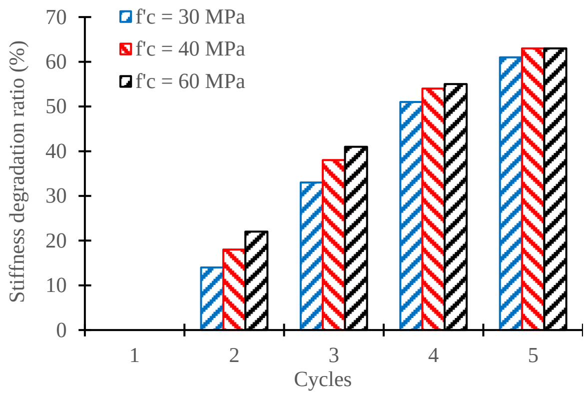

Fig. 15. Evolution of stiffness degradation ratio during early cyclic loading for various concrete strengths

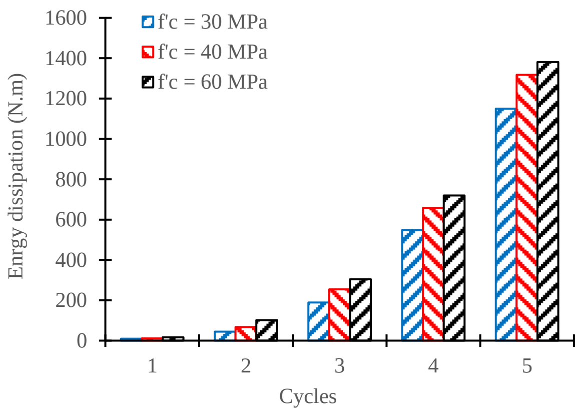

Fig. 16. Cumulative energy dissipation during early cyclic loading for various concrete strengths

These results confirm that in non-conforming joints, higher concrete strength may delay crack initiation but does not prevent significant stiffness degradation at early stages, consistent with findings reported in experimental studies.

Figure 16 reveals that cumulative energy dissipation (E_{cum}) increases slowly over the first five cycles, which is different from what Figure 15 shows, where stiffness rapidly decreases. Higher-strength concretes dissipate more energy in the first few cycles (≈16.6 N.m for f’c = 60 MPa versus 9.8 N.m for f’c = 30 MPa at cycle 1), and this difference stays the same through cycle 5 (≈ 1382 versus 1150 N.m). Consequently, although stiffness degradation tends to stabilize at comparable levels, energy dissipation continues to correlate with concrete strength, suggesting that the impact remains substantial on energy dissipation. The comparison between normalized stiffness degradation (K_{norm}) and normalized cumulative energy dissipation (E_{norm}), conducted for the three considered concrete compressive strengths (f'c), highlights the contrasting evolution of stiffness loss and energy dissipation, as shown in Figure 17.

While stiffness drops sharply from the very first cycles (drift ≤ 0.43%), energy dissipation remains nearly negligible, indicating an early loss of performance without significant absorption. At a drift of 0.57% (cycle 3), energy contribution becomes more pronounced, while stiffness continues to decline. The two curves intersect between 0.76% and 0.95% drift (cycles 4–5), which may be interpreted as a mechanical transition marking the progressive shift from quasi-elastic to inelastic response. This combined representation therefore highlights the complementary nature of the two parameters and emphasizes the importance of a coupled approach for a more refined characterization of early-stage damage.

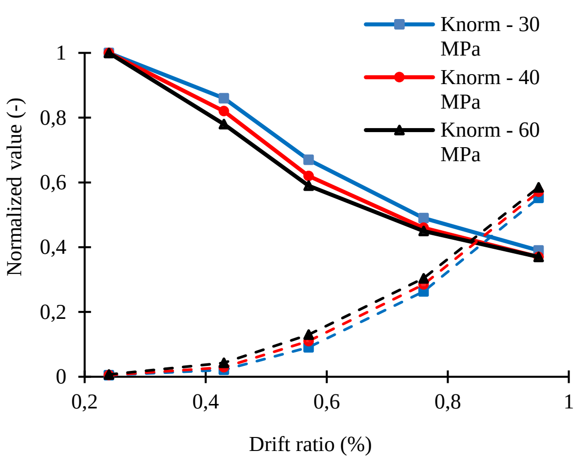

Fig. 17. Evolution of normalized stiffness degradation and cumulative energy dissipation during early cyclic loading for various concrete strengths

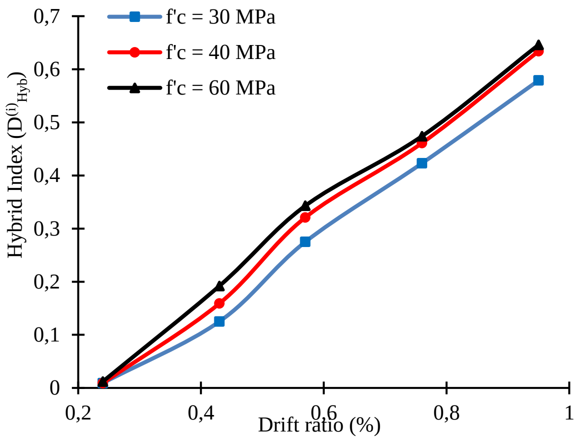

Fig. 18. Evolution of hybrid index (D_{Hybrid}) vs. drift ratio (%) during early cyclic loading for various concrete strengths

The hybrid indicator D_{Hybrid} exhibits a monotonic and steadily increasing trend from the very first cycles (Figure 18). In cycles 1 and 2 (drifts of 0.24% and 0.43%), values remain low (≈ 0.01 - 0.19 depending on f'c), reflecting limited dissipation despite an already initiated stiffness reduction. At cycle 3 (drift ≈ 0.57 %), the D_{Hybrid} index reaches 0.343 for f′c = 60 MPa, compared to 0.275 for f′c = 30 MPa. In cycles 4 and 5 (drifts of 0.76% and 0.95%), the indicator continues to rise and differences persist, with values ranging from 0.58 (30 MPa) to 0.65 (60 MPa). These results confirm that the effect of f′c begins in the first cycles and continues steadily as D_{Hybrid} progresses. This means that stronger concretes are more effective at promoting energy dissipation.

This study, limited to the first five loading cycles, highlights the interplay between stiffness degradation, energy dissipation, and the hybrid indicator D_{Hybrid}. The indicator effectively captures these coupled trends and the influence of concrete compressive strength, confirming that high-strength concretes, while initially stiffer, tend to exhibit lower ductility under cyclic loading [59, 60].

4.2 Effect of Beam Longitudinal Reinforcement Ratio: *ρ*

After examining the influence of concrete compressive strength, the following subsection evaluates the effect of the beam longitudinal reinforcement ratio on joint behavior. This ratio, denoted as ρ, is defined according to the BAEL 91 revised 1999 provisions [61]. A parametric variation of ρ is conducted using values of 0.5%, 0.83%, 1.0%, and 1.3%. The objective is to assess how changes in longitudinal reinforcement influence stiffness degradation, hysteretic energy dissipation, and the evolution of the D_{Hybrid} index during the early loading cycles.

Figure 19 shows the stiffness degradation ratio ($1-(K_i/K_0)$) over the first five cycles for different beam longitudinal reinforcement ratios. For all variants, stiffness loss occurs rapidly as early as the second cycle, representing approximately 26% for ρ = 0.5% and only 8% for ρ = 1.3%. In subsequent cycles, degradation continues: by the third cycle, stiffness loss reaches nearly 46% for the lowest-reinforced variant, compared with 19% for the most heavily reinforced one; by the fifth cycle, losses peak around 68% and 55% respectively. Increasing ρ therefore mitigates the initial stiffness degradation but does not prevent the overall loss of stiffness.

Figure 20 shows the evolution of cumulative energy dissipation (E_{cum}) for different beam longitudinal reinforcement ratios over the first five cycles. As early as the second cycle, clear differences emerge: the lightly reinforced variant ρ= 0.5% dissipates 71 N.m compared to only 25 N.m for ρ = 1.3%. The result shows that the first variant enters the inelastic regime earlier. This pattern continues through the fifth cycle, where the cumulative energy dissipation for ρ = 0.5% reaches 1327 N.m and for ρ = 1.3% it is 1143 N.m. The ρ = 1% variant exhibits better performance than the 1.3% case at cycle 4 (594 vs. 555 N.m) and at cycle 5 (1249.25 vs. 1142.51 N.m). This shows that the energy dissipation efficiency does not increase linearly with the reinforcement ratio, and that additional reinforcement could limit the activation of dissipative mechanisms. These results confirm that lightly reinforced beams dissipate more energy because they bend more, while heavily reinforced beams delay the activation of dissipative mechanisms, which is consistent with Figure 19, where they kept their stiffness longer.

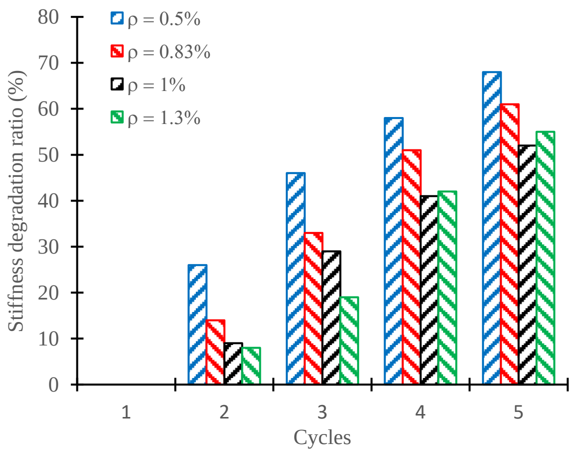

Fig. 19. Evolution of stiffness degradation ratio during early cyclic loading for various beam reinforcement ratios

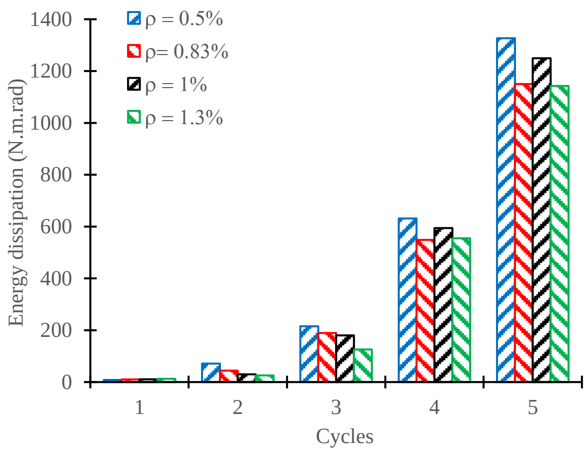

Fig. 20. Cumulative energy dissipation during early cyclic loading for various beam reinforcement ratios

The combined analysis of normalized stiffness degradation (K_{norm}) and normalized cumulative energy dissipation (E_{norm}), conducted for beam longitudinal reinforcement ratios (ρ) of 0.5%, 0.83%, 1.0%, and 1.3%, as illustrated in Figure 21, reveals two distinct behavioral phases over the first five cycles. Up to cycle 3, the response remains predominantly quasi-elastic: stiffness decreases rapidly, with a loss of about 26% for ρ = 0.5% compared to only 8 % for ρ = 1.3%, while energy dissipation remains very low (0.034 vs. 0.012). At Cycle 3, for a drift of 0.57 %, energy dissipation begins to accelerate (0.103 for 0.5 % vs. 0.060 for 1.3 %) while stiffness degradation continues (46% vs. 19%). From cycle 4 (drift ≈ 0.76%), a clear transition to a post-elastic regime is observed, with energy dissipation becoming increasingly significant. At this point, the least reinforced variant has already lost considerable stiffness (about 58%) while exhibiting substantial normalized energy dissipation (about 0.30). This step is when the post-elastic behavior starts to become clear. The most reinforced variant, on the other hand, shows a higher residual stiffness (about 42%) and a lower energy dissipation (about 0.27).

This result means that dissipative mechanisms take longer to activate. The least reinforced variant loses 68% of its stiffness by cycle 5 (drift ≈ 0.95%), while the most reinforced variant loses 55%. The normalized energy dissipation values are 0.64 and 0.55, respectively. As stiffness approaches its residual plateau, this evolution shows that energy dissipation becomes increasingly significant in the global response. These results support the idea that increasing ρ makes stiffness last longer and delays the activation of dissipative mechanisms, as illustrated in Figures 19 and 20.

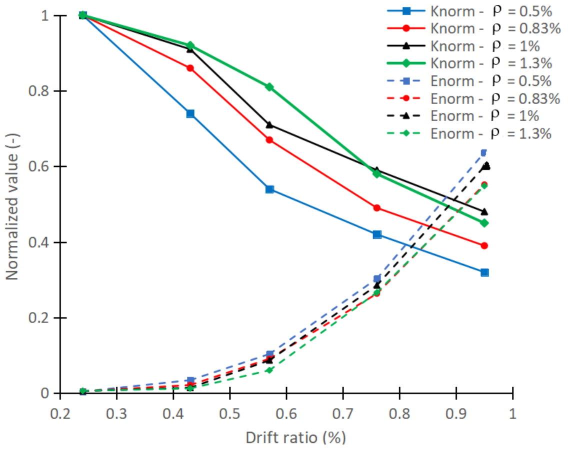

Fig. 21. Evolution of normalized stiffness degradation and cumulative energy dissipation during early cyclic loading for various beam reinforcement ratios

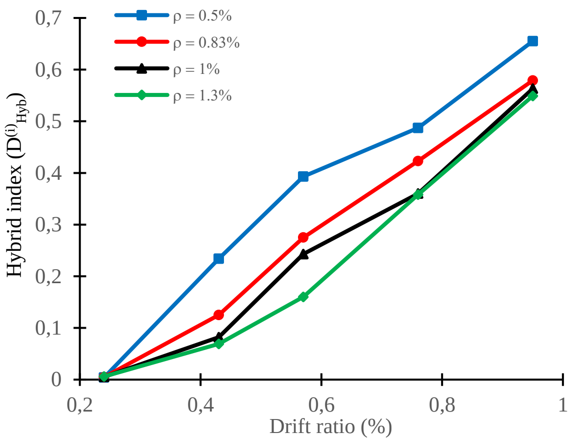

Fig. 22. Evolution of hybrid index (D_{Hybrid}) vs. drift ratio (%) during early cyclic loading for various beam reinforcement ratios

The hybrid index D_{Hybrid} increases monotonically over the first five cycles, reflecting a continuous progression of joint damage. The results illustrated in Figure 22 show that, for cycles 1 and 2, the values remain low (≈ 0.23 for ρ = 0.5% versus ≈ 0.07 for ρ = 1.3%), indicating that the damage is still dominated by the initial stiffness loss. The index grows faster after cycle 3, increasing from 0.16 to 0.39 (drift ≈ 0.57%). This means that the joint is beginning to activate energy-dissipating mechanisms. The trend continues in cycles 4 and 5, with a steady gap (0.66 versus 0.55). By synthesizing stiffness and energy contributions into a single indicator, D_{Hybrid} highlights the transition from quasi-elastic to post-elastic behavior and enables a clear comparison between reinforcement configurations. It thus is shown to be a relevant synthetic indicator for comparing damage evolution at low drift levels.

The joint evolution of stiffness degradation and energy dissipation marks a clear transition from stiffness-controlled behavior in the early cycles to energy-dominated response thereafter. The D_{Hybrid} indicator confirms that lightly reinforced joints reach higher damage levels at moderate drift ratios (≈ 1%). These results align with prior studies showing that higher reinforcement ratios enhance stiffness retention but require sufficient confinement to sustain ductility and energy dissipation [62, 63]. Similarly, Sabbahfar et al. [64] reported that deformed bars improve both stiffness stability and energy capacity compared with plain bars.

4.3 Effect of Joint Transverse Reinforcement Ratio: *Atr*

In addition to the beam longitudinal reinforcement ratio, the influence of joint transverse reinforcement is investigated to assess its role in confinement and cyclic response. The joint transverse reinforcement is deliberately imposed as a parameter representative of pre-code practices. The reference case corresponds to the absence of transverse reinforcement in the joint core (Atr_0), while configurations with 1 (Atr_1), 2 (Atr_2), and 3 stirrups (Atr_3) represent a progressive increase in confinement, with the case of 3 stirrups corresponding to the minimum requirement prescribed by the RPA 2024 [65].

Figure 23 shows that, for cycles 1–2 (low drifts), the stiffness response is only marginally affected by the amount of transverse reinforcement in the joint; the normalized residual stiffness data (K_i/K_0) are nearly superimposed. From cycles 3–4 onward, stiffness continues to decrease for all configurations, with no significant benefit from additional transverse reinforcement. At cycles 4–5 (moderate drifts), the differences remain minimal. Overall, within the studied drift range (≈ 1%), joint confinement does not significantly improve stiffness retention.

Figure 24 shows the evolution of cumulative energy dissipation for different levels of transverse reinforcement within the joint. Up to cycle 3, the curves remain very close, indicating that joint confinement has little influence on energy dissipation during the early stages of loading. Beginning with cycle 4, a small gap becomes visible, and the most restricted joint (Atr_3) loses slightly more energy. By cycle 5, the difference becomes more consistent, with Atr_3 reaching about 1205 N.m compared to roughly 1150–1158 N.m for the other configurations. These results suggest that transverse reinforcement has little influence on energy dissipation at low drifts. However, at moderate drifts, it contributes to a modest increase in hysteretic energy capacity. This behavior is consistent with the expected stabilizing effect of confinement on joint shear cracking.

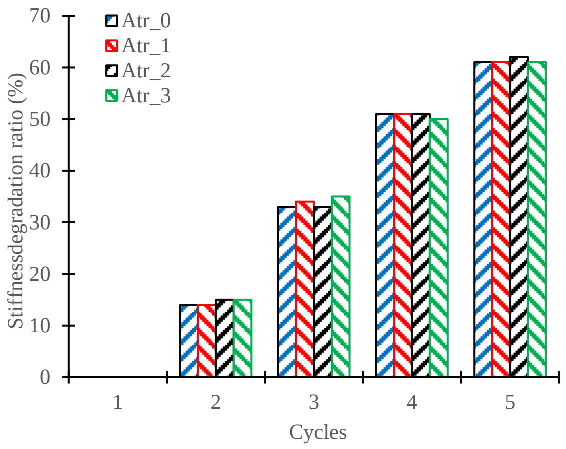

Fig. 23. Evolution of stiffness degradation ratio during early cyclic loading for various joint transverse reinforcement ratio

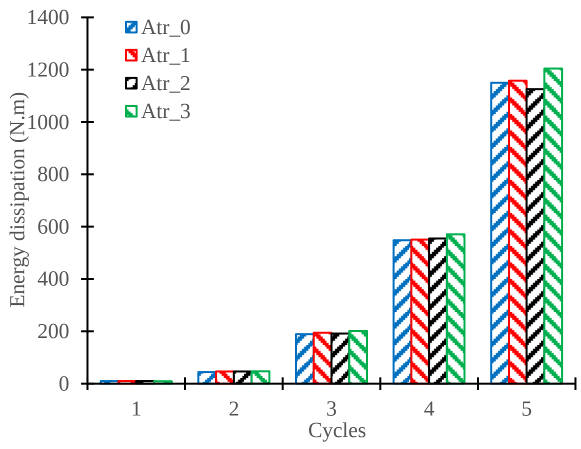

Fig. 24. Cumulative energy dissipation during early cyclic loading for various joint transverse reinforcement ratio

The combined analysis of normalized stiffness degradation (K_{norm}) and normalized cumulative dissipated energy (E_{norm}), conducted for different configurations of joint transverse reinforcement, as shown in Figure 25, reveals that the amount of transverse reinforcement within the joint has a limited influence on stiffness over the first five cycles. The (K_i/K_0) values remain very close across all configurations, around 0.85 by cycle 2 and converging toward 0.38–0.39 by cycle 5. In contrast, a slight but consistent separation is observed in the normalized energy from cycle 4 onward, with the most confined joint (three stirrup frames) systematically dissipating slightly more energy. This tendency is confirmed at cycle 5, where ($E_{cum,5}/E_{ref}$) reaches approximately 0.53 for the most confined joint compared to about 0.50 for the other configurations. This combined reading suggests that, at low to moderate drifts, joint confinement does not significantly improve stiffness retention but contributes to a modest increase in energy dissipation as cycles accumulate (cycles 4–5).

The hybrid index D_{Hybrid} shows steady growth across all transverse reinforcement configurations (Figure 26). In the first two cycles (drifts ≤ 0.43%), differences remain minor (≈ 0.126 for the unconfined joint vs. ≈ 0.139 for the most confined), confirming that early damage is governed mainly by stiffness loss. From cycle 3 (drift ≈ 0.57%), the most confined joint shows slightly higher values (0.29 vs. 0.27), indicating a more pronounced activation of dissipative mechanisms. This difference continues through cycles 4–5 (0.43 vs. 0.41), which means that confinement slightly speeds up energy dissipation while slowing down the process of getting very low residual stiffness. Overall, within the studied drift range (≤ 1%), transverse reinforcement does not fundamentally alter the damage mechanism, but promotes a more gradual and stable energy dissipation, consistent with the trends observed in Figures 23–25.

Within the studied drift range (≤ 1%), joint confinement does not significantly improve stiffness retention, as K_i/K_0 curves remain closely aligned for all configurations. However, a modest but consistent increase in cumulative energy dissipation is observed from cycles 4–5 for the most confined joint, which is also reflected by slightly higher D_{Hybrid} values. Similar observations reported in [66-68] indicate that confinement within the joint core, whether provided by transverse or diagonal reinforcement, primarily enhances energy dissipation and post-cracking stability.

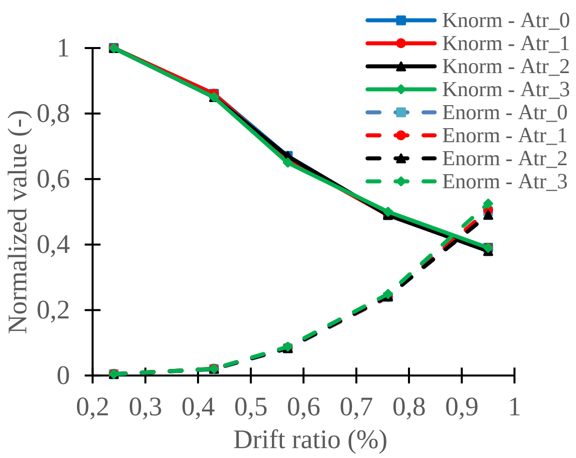

Fig. 25. Evolution of normalized stiffness degradation and cumulative energy dissipation during early cyclic loading for various joint transverse reinforcement ratio

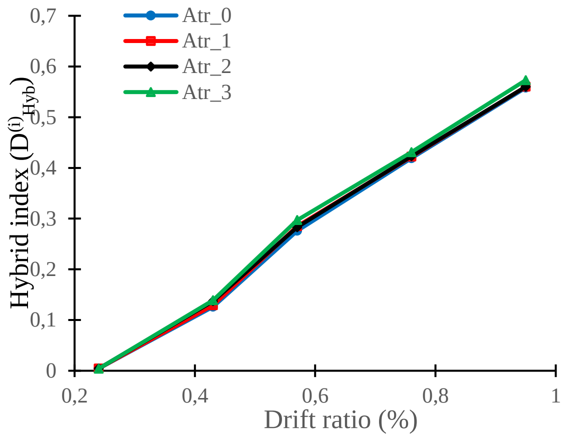

Fig. 26. Evolution of hybrid index (D_{Hybrid}) vs. drift ratio (%) during early cyclic loading for various joint transverse reinforcement ratio

5. Conclusions

This study investigated the seismic response of non-conforming exterior RC beam–column joints typical of pre-code Algerian constructions. Using a three-dimensional nonlinear finite element model developed in ANSYS, the analysis focused on the first five loading cycles to capture the onset of stiffness degradation and energy dissipation mechanisms. By combining these two parameters, a hybrid damage index (D_{Hybrid}) was proposed to provide an integrated assessment of early cyclic damage. The main findings can be summarized as follows:

- Stiffness degradation occurs rapidly during the first two cycles, whereas energy dissipation remains initially limited and becomes significant only from the third cycle onward, highlighting the high vulnerability of these joints in the early loading stage.
- The originality of this study lies in combining stiffness degradation and energy dissipation through a normalized dual-curve representation. This approach allows the identification of a critical intersection point that represents the threshold at which dissipative mechanisms progressively prevail over stiffness loss, marking the onset of post-elastic behavior. On this basis, a conceptual hybrid index (D_{Hybrid}) is proposed as a unified indicator for damage assessment.
- Increasing concrete compressive strength does not prevent early stiffness degradation; however, it results in higher cumulative energy dissipation from the first cycle. The hybrid index (D_{Hybrid}) consistently captures this dual and contrasting influence in early damage assessment.
- Higher beam longitudinal reinforcement ratios delay stiffness loss but reduce dissipative capacity, while lower ratios promote earlier energy dissipation. This trade-off is clearly reflected by the evolution of D_{Hybrid}.
- Within the investigated drift range (up to 1%) and early cycles, transverse reinforcement has a limited effect on stiffness retention but contributes modestly to stabilizing hysteretic energy dissipation, a trend also captured by D_{Hybrid}.
- The first loading cycles capture the onset of stiffness degradation and early dissipative mechanisms in RC beam–column joints. Concrete strength, beam longitudinal reinforcement, and joint confinement influence this initial stage in different ways, while D_{Hybrid} provides an integrated measure of early damage. This early-cycle perspective is particularly relevant for non-ductile structures, where damage accumulates rapidly and governs seismic vulnerability.

Future work will address the experimental validation of the proposed hybrid damage index and its application to different RC joint configurations.

Acknowledgement

The authors would like to express their gratitude to the Algerian government and the DGRSDT for the financial support granted as part of a scholarship program. Additionally, the technical support provided by the staff of the IMAC laboratory at EPFL, Switzerland is greatly appreciated.

References

[1] Davidovici, V. Séisme de Boumerdes – 21 mai 2003. Rapport préliminaire, Ministère de l'Habitat – Algérie, Dynamic concept, Juin, 2003. https://www.afps-seisme.org/rapports-de-missions-post-sismiques/2003-boumerdes-algérie

[2] Pampanin S, Calvi GM, Moratti M. Seismic behaviour of R.C. beam–column joints designed for gravity loads. Proceedings of the 12th European Conference on Earthquake Engineering (ECEE), London, UK, September, 2002.

[3] Pantelides CP, Hansen J, Nadauld J, Reaveley LD. Assessment of reinforced concrete building exterior joints with substandard details. PEER Report 2002/18, Pacific Earthquake Engineering Research Center, University of California, Berkeley, May, 2002. https://peer.berkeley.edu/sites/default/files/0218_c._pantelides_j._hansen_j._nadauld_l._reaveley.pdf

[4] Sezen H, Elwood KJ, Whittaker AS, Mosalam KM, Wallace JW, Stanton JF. Structural engineering reconnaissance of the august 17, 1999, kocaeli (izmit), Turkey. Earthquake. PEER Report 2000/09, Pacific Earthquake Engineering Research Center, College of Engineering, University of California, Berkeley, December, 2000. https://doi.org/10.13140/RG.2.1.1324.2483

[5] Günay MS, Mosalam KM. Structural engineering reconnaissance of the April 6, 2009, Abruzzo, Italy, earthquake, and lessons learned. PEER Report 2010/105, Pacific Earthquake Engineering Research Center, College of Engineering, University of California, Berkeley, April, 2010. https://peer.berkeley.edu/sites/default/files/web_peer10_105_m._selim_gnay_khalid_m._mosalam.pdf

[6] Durrani AJ, Wight JK. Behavior of interior beam–column connections under earthquake-type loading. ACI Journal, 1985; 82-30: 343–349. https://doi.org/10.14359/10341

[7] Ehsani MR, Wight JK. Effect of transverse beam and slab on the behavior of reinforced concrete beam-to-column connections. ACI Journal, 1985; 82(2): 188–195. https://doi.org/10.14359/10327

[8] Aycardi LE, Mander JB, Reinhorn AM. Seismic resistance of reinforced concrete frame structures designed only for gravity loads: Experimental performance of sub assemblages. Technical Report NCEER-92-0028, National Center For Earthquake Engineering Research, State University of New York at Buffalo, December, 1992. https://www.eng.buffalo.edu/mceer-reports/92/92-0028.pdf

[9] Hakuto S, Park R, Tanaka H. Seismic load tests on interior and exterior beam–column joints with substandard reinforcing details. ACI Structural Journal, 2000; 97(1): 11–25. https://doi.org/10.14359/829

[10] Clyde C, Pantelides CP, Reaveley LD. Performance-based evaluation of exterior reinforced concrete building joints for seismic excitation. PEER Report 2000/05. Pacific Earthquake Engineering Research Center, University of California, Berkeley, July, 2000. https://peer.berkeley.edu/sites/default/files/0005_c._clyde_c._pantelides_l._reaveley.pdf

[11] Tsonos AG. Effectiveness of CFRP-jackets and RC-jackets in post-earthquake and pre-earthquake retrofitting of beam-column subassemblages. Engineering Structures, 2008, 30(3): 777–793. https://doi.org/10.1016/j.engstruct.2007.05.008

[12] Le-Trung K, Lee K, Lee J, Lee DH, Woo S. Experimental study of RC beam–column joints strengthened using CFRP composites. Composites Part B: Engineering, 2010; 41(1): 76-85. https://doi.org/10.1016/j.compositesb.2009.06.005

[13] Kuang JS, Wong HF. Effects of beam bar anchorage on beam–column joint behaviour. Proceedings of the Institution of Civil Engineers – Structures and Buildings, 2006; 159(2): 115–124. https://doi.org/10.1680/stbu.2006.159.2.115

[14] Del Vecchio C, Di Ludovico M, Balsamo A, Prota A. Seismic retrofit of real beam–column joints using fiber-reinforced cement composites. Journal of Structural Engineering, 2018; 144(5): 04018026. https://doi.org/10.1061/(ASCE)ST.1943-541X.0001999

[15] Sonawane YN, Dubey S. Comparative analysis of seismic resilience: conventional vs. rectangular spiral reinforcement in joints. Research on Engineering Structures and Materials. 2024;10(4):1733-1758. http://dx.doi.org/10.17515/resm2024.494st1019rs

[16] Shaaban IG, Seoud OA. Experimental behavior of full-scale exterior beam–column space joints retrofitted by ferrocement layers under cyclic loading. Case Studies in Construction Materials, 2018; 8: 61-78. https://doi.org/10.1016/j.cscm.2017.11.002

[17] Lim C, Jeong Y, Kim J, Kwon M. Experimental study of reinforced concrete beam–column joint retrofitted by CFRP grid with ECC and high strength mortar. Construction and Building Materials, 2022; 340: 127694. http://doi.org/10.1016/j.conbuildmat.2022.127694

[18] Araby MZ, Rizal S, Abdullah, Afifuddin M, Hasan M. Deformation capacity of RC beam–column joints strengthened with ferrocement. Sustainability, 2022; 14(8): 4398. https://doi.org/10.3390/su14084398
[19] Helal Y, Garcia R, Imjai T, Aosai P, Guadagnini M, Pilakoutas K. Seismic behaviour of exterior RC beam–column joints repaired and strengthened using post-tensioned metal straps. Bulletin of Earthquake Engineering, 2024; 22: 3261–3286. https://doi.org/10.1007/s10518-024-01904-1
[20] Golias E, Karayannis C. Effect of C-FRP (carbon fiber reinforced polymer) rope and sheet strengthening on the shear behavior of RC beam-column joints. Fibers, 2025; 13(9): 113. https://doi.org/10.3390/fib13090113
[21] Paulay T, Priestley MJN. Seismic design of reinforced concrete and masonry buildings. Wiley-Interscience, New York, USA, 1992.
[22] Biddah A, Ghobarah A. Modelling of shear deformation and bond slip in reinforced concrete joints. Structural Engineering and Mechanics, 1999; 7(4): 413–432. https://doi.org/10.12989/sem.1999.7.4.413
[23] Hwang SJ, Lee HJ. Analytical model for predicting shear strengths of exterior reinforced concrete beam–column joints for seismic resistance. ACI Structural Journal, 1999; 96(5): 846–858. https://doi.org/10.14359/739
[24] Lowes LN, Mitra N, Altoontash A. A beam–column joint model for simulating the earthquake response of reinforced concrete frames. PEER Report 2003-10, Pacific Earthquake Engineering Research Center, University of California, Berkeley, CA, February, 2004. https://peer.berkeley.edu/sites/default/files/0310_l._lowes_n._mitra_a._altoontash.pdf
[25] Mitra N, Lowes LN. Evaluation, calibration, and verification of a reinforced concrete beam–column joint model. Journal of Structural Engineering, 2007; 133(1): 105–120. https://doi.org/10.1061/(ASCE)0733-9445(2007)133:1(105)
[26] Celik OC, Ellingwood BR. Modeling beam-column joints in fragility assessment of gravity load designed reinforced concrete frames. Journal of Earthquake Engineering, 2008; 12(3): 357–381. https://doi.org/10.1080/13632460701457215
[27] Park S, Mosalam KM. Shear strength models of exterior beam-column joints without transverse reinforcement. PEER Report 2009/106, Pacific Earthquake Engineering Research Center, University of California, Berkeley. CA, November, 2009. https://peer.berkeley.edu/sites/default/files/web_peer9106_sangjoon_park_and_khalid_m._mosalam.pdf
[28] Le-Trung K, Lee K, Shin M, Lee J. Analytical assessment and modeling of RC beam–column connections strengthened with CFRP composites. Composites Part B: Engineering, 2011; 42(7): 1786–1798. https://doi.org/10.1016/j.compositesb.2011.07.002
[29] LaFave JM, Kim J. Joint shear behavior prediction for RC beam–column connections. International Journal of Concrete Structures and Materials, 2011; 5(1): 57–64. https://doi.org/10.4334/IJCSM.2011.5.1.057
[30] Mosallam A, Allam K, Salama M. Analytical and numerical modeling of RC beam–column joints retrofitted with FRP laminates and hybrid composite connectors. Composite Structures, 2019; 214: 486–503. https://doi.org/10.1016/j.compstruct.2019.02.032
[31] Panto B, Caddemi S, Calio I, Spacone E. A 2D beam–column joint macro-element for the nonlinear analysis of RC frames. Earthquake engineering structural dynamics, 2020; V 50(3): 935-954. https://doi.org/10.1002/eqe.3375
[32] Gombosuren D, Maki T. Prediction of Joint Shear Deformation Index of RC Beam–Column Joints. Buildings, 2020; 10: 176. https://doi.org/10.3390/buildings10100176
[33] Grande E, Imbimbo M, Napoli A, Nittif R, Realfonzo R. A nonlinear macro-model for the analysis of monotonic and cyclic behaviour of exterior RC beam–column joints. Frontiers in materials, 2021; 8: 719716. http://doi.org/10.3389/fmats.2021.719716
[34] Irreño Palomo IR, Frappa G, de Almeida LC, Trautwein LM, Pauletta M (). Analytical and numerical models to determine the strength of RC exterior beam–column joints retrofitted with UHPFRC. Engineering Structures, 2024; 312: 118244. https://doi.org/10.1016/j.engstruct.2024.118244
[35] Kalogeropoulos G, Tsonos AD, Iakovidis P (). Hysteresis behavior of RC beam–column joints of existing substandard RC structures subjected to seismic loading – Experimental and analytical investigation. Buildings, 2024; 14(6): 1609. https://doi.org/10.3390/buildings14061609
[36] Goto Y. Joh O. Shear resistance of RC interior eccentric beam-column joints. Proceedings of the 13th World Conference on Earthquake Engineering (WCEE 2004), Vancouver, B.C., Canada, August, 2004. https://www.iitk.ac.in/nicee/wcee/article/13_649.pdf
[37] Ibrahim HH. Elbadry M. Nonlinear 3d finite element analysis of exterior beam-column joints reinforced with double-headed studs for shear resistance under cyclic loading. In Proceedings of the Canadian Society for Civil Engineering / Structural Specialty Conference, Quebec City, Quebec, Canada, June, 2008.
[38] Eslami A, Dalalbashi A. Ronagh HR. On the effect of plastic hinge relocation in RC buildings using CFRP. Composites Part B: Engineering, 2013; 52: 350-361. https://doi.org/10.1016/j.compositesb.2013.04.025
[39] Baji H, Eslami A. Ronagh HR. Development of a nonlinear FE modelling approach for FRP-strengthened RC beam-column connections. Structures, 2015; 3: 272-281. http://dx.doi.org/10.1016/j.istruc.2015.06.003
[40] Venkatesan B, Ilangovan R, Jayabalan P, Mahendran N, Sakthieswaran N. Finite element analysis (FEA) for the beam-column joint subjected to cyclic loading was performed using ANSYS. Circuits and Systems, 2016; 7: 1581-1597. http://dx.doi.org/10.4236/cs.2016.78138

[41] Laseima SY, Mutalib AA, Osman SA, Hamid NH. Strengthening of deficient exterior RC beam-column joints using basalt fibre reinforced polymer sheets. Journal of Engineering Science and Technology, 2021, 16(5):3687–3711. https://jestec.taylors.edu.my/Vol%2016%20Issue%205%20October%202021/16_5_06.pdf
[42] Al-Rousan RZ, Alkhawaldeh A. Numerical simulation of the influence of bond strength degradation on the behavior of reinforced concrete beam-column joints externally strengthened with FRP sheets. Case Studies in Construction Materials, 2021; 15: e00567. https://doi.org/10.1016/j.cscm.2021.e00567
[43] Kytinou VK, Kosmidou PMK. Chalioris CE. Numerical analysis exterior RC beam-column joints with CFRP bars as beam's tensional reinforcement under cyclic reversal deformations. Applied Sciences, 2022; 12(15): 7419. https://doi.org/10.3390/app12157419
[44] Fayaz Q, Kaur G, Bansal PP. Numerical modelling of an exterior RC beam-column joint subjected to cyclic loading strengthened using UHPFRC and CFRP. In ASPS Conference Proceedings, 2022, 1(3): 891-900. https://doi.org/10.38208/acp.v1.599
[45] Marie HS, Abu el-Hassan K, Almetwally EM, El-Mandouh, MA. Joint shear strength prediction of beam-column connections using machine learning via experimental results. Case Studies in Construction Materials, 2022; 17: e01463. https://doi.org/10.1016/j.cscm.2022.e01463
[46] Zhuang ML, Cheng J, Fei D, Sun C, Wang Z, Chen B, Qiao Y. Numerical simulation study on the seismic performance of prefabricated fiber-reinforced concrete beam–column joints with grouted sleeve connections. International Journal of Concrete Structures and Materials, 2024; 18: 26. https://doi.org/10.1186/s40069-024-00671-2
[47] Sayed Ahmed MM, El-Zoughiby ME, Abdelwahed BS. Numerical investigation of retrofitting techniques for substandard exterior reinforced concrete beam–column joints. Innovative Infrastructure Solutions, 2025, 10: 233. https://doi.org/10.1007/s41062-025-02017-7
[48] Maulana H, Syaifa L, Nabila WU, Thamrin R, Kurniawan R. Finite element model of reinforced concrete interior beam–column joints subjected to cyclic loading. In 2nd ICDMM, E3S Web of Conferences, December, 2023. https://doi.org/10.1051/e3sconf/202346415007
[49] Sabbahfar P, Melo J, Costa A, Varum H, Rodrigues H. Cyclic behavior of seismically non-conforming interior reinforced concrete beam–column joints. Buildings, 2025; 15(2): 202. https://doi.org/10.3390/buildings15020202
[50] Prakash RS, Parthasarathi N. Experimental and numerical study on FRP-rehabilitated RC beam-column joints at high temperature with artificial neural network. Scientific Reports, 2025, 15: 30016. https://doi.org/10.1038/s41598-025-16055-9
[51] ANSYS Inc. ANSYS Mechanical APDL Basic Analysis Guide. Release 15.0. Canonsburg (PA): ANSYS Inc., 2013.
[52] Willam KJ, Warnke EP. Constitutive model for the triaxial behavior of concrete. International Association For Bridge And Structural Engineering Proceedings, 1-30, Bergamo, Italy, May, 1975.
[53] Kachlakev, D, Miller T, Yim S, Chansawat K, Potisuk T. Finite element modeling of reinforced concrete structures strengthened with FRP laminates. Oregon Department of Transportation Research Group, Final report SPR 316, Salem, OR , May, 2001. https://rosap.ntl.bts.gov/view/dot/23018/dot_23018_DS1.pdf
[54] Gencoglu M, Mobasher B. The strengthening of the deficient RC exterior beam-column joints using CFRP for seismic excitation. In Proceedings of the Third International Conference on Structural Engineering, Mechanics and Computation, Cape Town, South Africa, 1993- 1998, September, 2007. https://scholar.google.com/scholar?oi=bibs&cluster=12338001808477370724&btnI=1&hl=en
[55] Ronagh HR, Baji H. On the FE modeling of FRP-retrofitted beam–column subassemblies. International Journal of Concrete Structures and Materials, 2014; 8(2): 141-155. https://doi.org/10.1007/s40069-013-0047-y
[56] Suprobo P, Tambusay A, Suryanto B, Nelson JJM. Seismic performance of ordinary and damage-tolerant concrete beam-column joints under reversed cyclic loading. IOP Conference Series: Earth and Environmental Science, 2023, 1244, 012011. IOP Publishing. https://doi.org/10.1088/1755-1315/1244/1/012011
[57] Tsonos AD, Kalogeropoulos G, Iakovidis P, Bezas MZ, Koumtzis M. Seismic performance of RC beam–column joints designed according to older and modern codes: An attempt to reduce conventional reinforcement using steel fiber reinforced concrete. Fibers, 2021; 9(7): 45. https://doi.org/10.3390/fib9070045
[58] Park YJ, Ang AHS. Mechanistic seismic damage model for reinforced concrete. Journal of Structural Engineering, 1985; 111(4): 722–739. https://doi.org/10.1061/(ASCE)0733-9445(1985)111:4(722)
[59] Atta AEN, Taher SEDF, Khalil AHA, El-Metwally SED, . Behaviour of reinforced high-strength concrete beam–column joint. Part 1: Experimental investigation. Structural Concrete, 2003; 4(4): 175-183. https://doi.org/10.1680/stco.2003.4.4.175
[60] Chen X, Wu J, Shang K, Ning Y, Bai L. Investigation of the deformation and failure characteristics of high-strength concrete in dynamic splitting tests. International Journal of Concrete Structures and Materials, 2022; 16: 58. https://doi.org/10.1186/s40069-022-00548-2
[61] Règles BAEL 91 révisées 99. Règles techniques de conception et de calcul des ouvrages et constructions en béton armé suivant la méthode des états limites. DTU P 18-702, CSTB, Paris, Février 1999. https://www.sodibet.com/telechargement/BAEL%2091%20R%2099.pdf?utm_source=chatgpt.com
[62] Merati W, Widagdo P. The effects of column stirrup and longitudinal beam reinforcement on exterior beam-column joint under cyclic loading. Transactions on the Built Environment, WIT Press, 1996; 17: 217 - 226. https://doi.org/10.2495/CMT960221

[63] Feng J, Wang S, Meloni M, Zhang Q, Yang J, Cai J. Seismic behavior of RC beam column joints with 600 MPa high strength steel bars. Applied Sciences, 2020; 10(13): 4684. https://doi.org/10.3390/app10134684
[64] Sabbahfar P, Melo J, Costa A, Varum H, Rodrigues H. Cyclic behavior of seismically non-conforming interior reinforced concrete beam–column joints. Buildings, 2025; 15(2): 202. https://doi.org/10.3390/buildings15020202
[65] RPA 2024. Règles Parasismiques Algériennes. Document Technique Réglementaire D.T.R. - B.C. 2.48, Ministère de l'Habitat, de l'Urbanisme et de la Ville, Algérie, 2024. https://www.gcalgerie.com/regles-parasismiques-algeriennes-rpa-2024/
[66] Joh O, Goto Y, Shibata T. Influence of transverse reinforcement in joints and beam ends on the behavior of R/C beam-column subassemblages. Bulletin of the Faculty of Engineering, Hokkaido University, 1988; 145: 29-39. http://hdl.handle.net/2115/42176
[67] Wongkaew A. Experimental investigation of exterior reinforced concrete beam-column connections subjected to reversal loading. Trends in Sciences, 2022; 19(20): 6217. https://doi.org/10.48048/tis.2022.6217
[68] Shen X, Li B, Chen YT, Tizani W. Experimental and numerical study on reinforced concrete beam-column joints with diagonal bars: Effects of bonding condition and diameter. Structures, 2022; 37: 905-918. https://doi.org/10.1016/j.istruc.2022.01.050